



Chemphys Perspective

Dynamical mechanism of charge separation by photoexcited generation of proton–electron pairs in organic molecular systems. A nonadiabatic electron wavepacket dynamics study[☆]

Kentaro Yamamoto, Kazuo Takatsuka*

Department of Basic Science, Graduate School of Arts and Sciences, The University of Tokyo, Komaba, 153-8902 Tokyo, Japan

ARTICLE INFO

Article history:

Received 19 April 2016

In final form 23 May 2016

Available online 9 June 2016

ABSTRACT

In this perspective article, we review, along with presenting new results, a series of our theoretical analyses on the excited-state mechanism of charge separation (proton–electron pair creation) relevant to the photoinduced water-splitting reaction ($2\text{H}_2\text{O} \rightarrow 4\text{H}^+ + 4\text{e}^- + \text{O}_2$) in organic and biological systems, which quite often includes Mn clusters in various molecular configurations. The present mechanism is conceived to be universal in the triggering process of the photoexcited water splitting dynamics. In other words, any Mn-based catalytic charge separation is quite likely to be initiated according to this mechanism. As computationally tractable yet realistic models, we examine a series of systems generally expressed as $\text{X}-\text{Mn}-\text{OH}_2 \cdot \text{A}$, where $\text{X}=(\text{OH}, \text{Ca}(\text{OH})_3)$ and $\text{A}=(N\text{-methylformamidine, guanidine, imidazole or ammonia cluster})$ in terms of the theory of nonadiabatic electron wavepacket dynamics. We first find both an electron and a proton are simultaneously transferred to the acceptors through conical intersections upon photoexcitation. In this mechanism, the electron takes different pathways from that of the proton and reaches the densely lying Rydberg-like states of the acceptors in the end, thereby inducing charge separation. Therefore the presence of the Rydberg-like diffused unoccupied states as an electron acceptor is critical for this reaction to proceed. We also have found another crucial nonadiabatic process that deteriorates the efficiency of charge separation by rendering the created pair of proton and electron back to the originally donor site through the states of d-d band originated from Mn atom. Repetition of this process gradually annihilates the created pair of proton and electron in a way different from the usual charge recombination process. We address this dynamics by means of our proposed path-branching representation. The dynamical roles of a doped Ca atom are also uncovered, which are relevant to controlling the pathways of electron flow and moreover to reduction of the annihilation dynamics of proton–electron pair.

© 2016 The Authors. Published by Elsevier B.V. This is an open access article under the CC BY-NC-ND license (<http://creativecommons.org/licenses/by-nc-nd/4.0/>).

1. Introduction

Photoinduced charge separation is the triggering key process to convert photon energy into other forms. The relevant mechanism in solid state materials, as in the studies on the solar cells, is known to be basically photoexcitation of electrons from the covalent states to conduction bands, resulting in the creation of an electron–hole pair. In organic and biological systems, charge separation is meant to be mainly the creation of pairs of isolated electrons and protons, each

of which is recycled in photochemistry to fix CO_2 and in giving birth to O_2 molecules from water. Thus the mechanisms of these two types of charge separation are totally different. We herein study the mechanism of very initial-stage dynamics of the photoinduced creation of electron–proton pair.

We stress that the present study is just concerned with the initial dynamics of proton–electron pair creation in excited states and is not intended to the analyses of the entire processes of the water splitting (oxidation of water), symbolically written down as



This simply looking chemical formula is actually very much involved [1–5]. Although the dynamical mechanism we are going to present here should be highly relevant to the charge separation in biological systems such as that in the photosystem II (PSII) in natural photosynthesis, we persist to perform the following

* This work was supported in part by a Grant-in-Aid for Basic Science from the Ministry of Education, Culture, Sports, Science and Technology of Japan (15H05752).

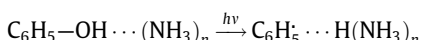
* Corresponding author at: Fukui Institute for Fundamental Chemistry, Kyoto University, Nishi-hiraki-cho 34-4, Takano, Sakyo-ku, Kyoto 606-8103, Japan.

E-mail addresses: kyamamoto@fukui.kyoto-u.ac.jp (K. Yamamoto), kaztak@fukui.kyoto-u.ac.jp (K. Takatsuka).

analyses in this article within a general theory of photochemistry. In doing so, we apply the method of full-dimensional nonadiabatic electron wavepacket dynamics, whereby we explicitly track the real-time dynamics of both electrons and protons that are collectively transferred to acceptors. The mechanism is illustrated in computationally tractable yet realistic molecular systems containing Mn, Ca, and H₂O.

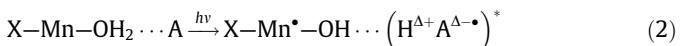
Technical application of water splitting is of course to the design of efficient photocatalysts for charge separation to produce hydrogen and oxygen molecules [6,7]. Mn-based materials are particularly well studied [8–11], mainly because they can be directly compared with the oxygen-evolving complex (Mn₄CaO₅ [12,13]) embedded in PSII. Moreover, Mn is earth abundant and less toxic than the other more active catalysts such as Os and Ru complexes [7].

In a series of fundamental studies on the role of conical intersection, Domcke and his coworkers studied the $\pi-\pi^*$ transition of a phenol that is hydrogen bonded to ammonia clusters. It serves as a physicochemical model to investigate a process to deactivate DNA bases to the ground state without photoinduced damage. They theoretically identified the initiation process with the excited-state hydrogen atom migration from the phenol to the ammonia clusters [14,15].



Stimulated by the relevant experiments on the above phenol plus ammonia clusters by Miyazaki and Fujii, in which the time scales of proton and electron dynamics are detected to be mutually different [16], Nagashima and Takatsuka performed theoretical calculations based on the nonadiabatic electron wavepacket dynamics [17]. They reconsidered the scenario about the pathways of electrons and protons, and found that an electron wavepacket actually undergoes nonadiabatic interaction to jump from the phenol to the Rydberg-like states of the ammonia clusters through conical intersections. On the other hand, the proton shifts along a different path as if it was in the electronic ground state. The proton thus transferred triggers proton-relay in the ammonia clusters. The separated charge remains long in the ammonia clusters before recombination through the other conical intersections leading down to the ground state.

In the present paper, we show that the above mentioned mechanism involving the Rydberg-like states is not peculiar to the dynamics of preventing photoinduced damage of DNA, but is far more ubiquitous as a mechanism of charge separation. A model reaction in which we are going to scrutinize as the fundamental mechanism of charge separation is generally represented as



in which X = (OH or Ca(OH)₃) and A = (*N*-methylformamidine, guanidine, imidazole, or ammonia cluster). The symbols “ \cdots ”, “ \bullet ”, and “ * ” indicate hydrogen bond, unpaired electron (radical), and excited electronic state, respectively. H ^{$\Delta+$} indicates proton with a partial positive charge to the extent of around 0.5e, while A ^{$\Delta-\bullet$} means an anion radical of the partial charge of the magnitude to the extent of ca. -0.5e. X denotes an arbitrary subsystem (or functional group), but is chosen to keep the system simple and stable. A serves as an electron-proton acceptor that has low-lying Rydberg-like excited states. Incidentally, each entry of A can be regarded as a part of a positively charged proteinogenic amino acid. X-Mn-OH₂ is regarded as one of the simplest units in which we consider the water-splitting [Eq. (1)] catalyzed by Mn oxides [8–11]. For every combination of A and X, we have commonly identified the same dynamical mechanism of coupled proton-electron transfer (simply referred to as CPET hereafter), where the proton and the electron pass through their own different

pathways to reach spatially different places. CPET thereby induces charge separation as $(\text{H}^{\Delta+}\text{A}^{\Delta-\bullet})^*$. Due to the space limitation, we highlight only the cases with A = *N*-methylformamidine as represented in Fig. 1, but the other A's make no qualitative difference. In what follows the transferred H atom in the present mechanism is referred to as H^T to be distinguished from the other nonreactive H atoms.

Nonadiabatic interaction among the excited states plays a key role in the mechanism of the dynamics of Eq. (2). Schematic representation for the case of X = OH is shown in Fig. 2. That of X = Ca(OH)₃ is essentially the same. It takes ~100 fs for the charge separation after the photoexcitation to finish. Even before photoexcitation, the system in its vibronic ground state (Fig. 2(a)) bears a small number of radical electrons (about 0.5e) on the electron donor (X-Mn-OH₂) due to electron correlation, which is reflected in the double excitation configurations in configuration interactions calculations. Then the electronic state is photoexcited to generate more radical electrons (actually biradical) on the donor (see the position (b) in Fig. 2). Note that right after the photoexcitation the Rydberg-like states of the acceptor (A) have no significant contribution, since direct photoexcitation to the Rydberg-like states is practically forbidden due to their small oscillator strength. After bouncing motion of OH^T in the (b) area of Fig. 2, CPET begins to take place. It involves nonadiabatic interaction in the way to induce electron transfer to the Rydberg-like states (the point (c) in Fig. 2). While the electron moves circularly, the proton is shifted almost linearly to reach different places from each other. Finally, an asymptotic biradical state is driven to the point (d) in Fig. 2.

Various theoretical studies have been made on coupled electron and proton transfer reactions in various different contexts such as protein functioning and the rate processes of proton-coupled electron transfer [18–25]. However, studies on electron dynamics for the mechanism of photoinduced charge separation in those catalytic molecular systems have not been published, to the best of our knowledge.

The above basic mechanism was reported earlier in a short communication [26]. In addition to the very core part of the theory presented in it, we herein discuss more about the relevant molecular orbitals and the ground-state dynamics, which is confirmed not to induce the charge separation dynamics. Besides a new channel of dynamics is reported that annihilates thus created pair of proton and electron through the d-d band states inherent to the Mn atom. To examine the role of the doping of Ca atom, we here study the role of X = Ca(OH)₃.

The present paper is presented as follows: In Section 2 we first briefly describe the notion and method to distinguish proton transfer and hydrogen atom migration from the view point of electron dynamics. The distinction between them is critically important to understand the essential characteristics of the dynamical mechanism of charge separation due to the generation of proton-electron pair. Section 3 is the heart of the paper, presenting precisely the catalytic mechanism by nonadiabatic electron dynamics for the creation of proton-electron pair from water molecule. Not only the mechanism of charge separation is clarified but also a channel of annihilation of thus created proton-electron pair is found. The role of Ca atom doped in the catalyses is also scrutinized. This paper conclude in Section 4 with some remarks.

2. Electron dynamical mechanisms of proton transfer and hydrogen migration

Towards the final goal of the novel excited-state mechanism of triggering the charge separation (proton-electron pair creation) dynamics of photoinduced water-splitting reaction, we need to clarify the dynamics of proton transfer in the ground states and

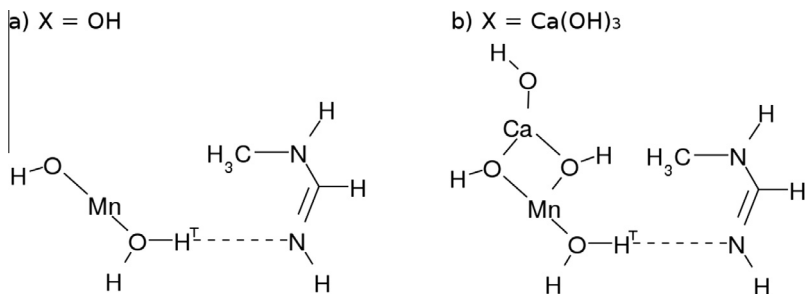


Fig. 1. Chemical structures of the model system $X\text{-Mn-OH}_2\cdots\text{A}$, where $X = (\text{OH or } \text{Ca}(\text{OH})_3)$ and $\text{A} = \text{N-methylformamidine}$. The proton transfer in the present mechanism takes place between O and the lone pair on the N atom of $\text{O}-\text{H}^{\text{T}}\cdots\text{N}$ bonds. The transferred H atom is referred to as H^{T} . The optimized structures are not planar but a little twisted along the $\text{O}-\text{H}^{\text{T}}\cdots\text{N}$ bonds.

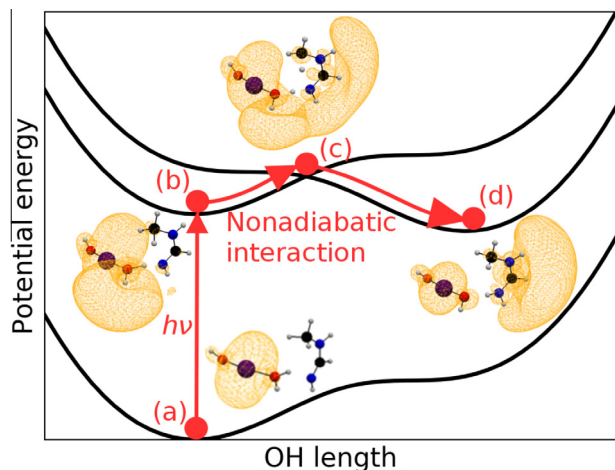


Fig. 2. Schematic (one-dimensionally reduced and very simplified) representation of the present mechanism of charge separation with spatial distribution of unpaired electron density. The case for $X = \text{OH}$ and $\text{A} = \text{N-methylformamidine}$ in Eq. (2) is illustrated just as an example. Note that there are actually many other quasidegenerate excited states mainly arising from the Rydberg-like states.

hydrogen atom migration in excited states. Extensive studies on the general theory of coupled electron and proton transfer have been made in the literature within the framework of traditional quantum chemistry based on the notion of static electronic states and the relevant potential energy surfaces [18–25]. In particular, Ref. [23] is relevant to the discussion made in this section. Seeming to be already clear, coupled proton-electron dynamics should be revisited from a view point of nonadiabatic electron dynamics.

2.1. Concerted reaction and radical reaction in spin singlet states

Fukui's frontier orbital theory and the Woodward–Hoffmann rule for the conservation of orbital symmetry in chemical reactions had chemists recognize how critically important the roles of quantum phases (actually orbital phases) are. Indeed, the Woodward–Hoffmann rule gives the notion of allowed and forbidden reactions in terms of the manifestation of the orbital phases with respect to molecular geometrical symmetry. The distinction between the allowed and forbidden reactions is essential also in order to distinguish proton transfer and hydrogen atom migration.

Cyclic addition reaction between 1,3-butadiene and ethylene, the so-called Diels–Alder reaction is a textbook material to illustrate the symmetry allowed reaction. HOMO (highest occupied molecular orbital) of 1,3-butadiene and LUMO (lowest unoccupied MO) of ethylene can form a new molecular orbital for the super-molecule, and likewise LUMO of 1,3-butadiene and HOMO of ethylene can also

form another new molecular orbital. Thus a cyclic addition can be achieved smoothly in a concerted way. The occupation number of these newly formed molecular orbitals are kept to about two throughout the reaction and hence even the RHF (restricted Hartree–Fock method) with a single determinant composed of doubly occupied molecular orbitals can successfully describe the entire reaction process. This type of reactions is therefore called concerted reaction.

One of the simplest forbidden reactions is thermal cyclic addition reaction between ethylene and ethylene. In this reaction, the phases between HOMO and LUMO cannot match to directly form new molecular orbitals, and thereby the simple RHF description fails in describing the smooth state-change. Methodologically the difficulty is circumvented by using the linear combination of plural Slater determinants as in the method of configuration interaction and one obtains a potential energy surface smoothly connected but with a high barrier. The potential energy surfaces thus reproduced with configuration interaction calculations for the ground state and the first excited state come close to each other in the energy coordinate in the vicinity of the top of the energy barrier. Quantum wavefunctions for nuclear motion undergo bifurcation to branch into two pieces running on the potential surfaces with a probability amplitude determined quantum mechanically depending on the intensity of the nuclear kinematic coupling elements and the velocity of the wavepackets passing through this region. The nonadiabatic transition thus dominates the reaction probability in forbidden reactions and excited state dynamics. The concerted reaction is virtually free from such nonadiabatic transition.

Question is how one can distinguish the electronic states between the concerted and forbidden reactions. In the forbidden reactions the smooth formation of the doubly occupied molecular orbitals is prohibited, and instead the so-called radicals are created on the way of reactions. In the ethylene–ethylene reaction, for instance, tetra radicals are tentatively created, each of which is centered on one of the four carbon atoms. These tentative radical formation and its spatial distribution can be monitored with the unpaired electron density $D(\mathbf{r})$, which is defined as

$$D(\mathbf{r}) = 2\rho(\mathbf{r}, \mathbf{r}) - \int d\mathbf{r}' \rho(\mathbf{r}, \mathbf{r}') \rho(\mathbf{r}', \mathbf{r}), \quad (3)$$

where $\rho(\mathbf{r}, \mathbf{r}')$ is the first order spinless density matrix in the coordinate representation [27]. It can be also expressed as

$$D(\mathbf{r}) = \sum n_i (2 - n_i) |\lambda_i(\mathbf{r})|^2, \quad (4)$$

where $\lambda_i(\mathbf{r})$ are the natural orbitals, which diagonalize the representation matrix of $\rho(\mathbf{r}, \mathbf{r}')$, and n_i are their associated occupation numbers. It is immediately observed that the vacant natural orbitals $n_i = 0$ and doubly occupied ones having $n_i = 2$ make no contribution to $D(\mathbf{r})$, while the singly occupied (radical-like) natural

orbitals gives the largest value to $D(\mathbf{r})$. In the concerted reactions as in the Diels–Alder reaction of 1,3-butadiene and ethylene, the total number of unpaired electrons counted as

$$N_u = \int D(\mathbf{r}) d\mathbf{r} \quad (5)$$

should be kept almost zero throughout the reaction. On the other hand, if purely tetra radical state is created in ethylene-ethylene reaction, N_u should amount to 4.

$D(\mathbf{r})$ is therefore utilized to clarify the difference between proton transfer and hydrogen atom transfer, since proton transfer in the ground state is generally concerted reaction, while hydrogen atom transfer occurs in electronically excited states in general, where hydrogen atom radical is created.

2.2. Hydrogen atom migration and radical creation in excited states

In the proton transfer dynamics in the ground state, which is symbolically written as



it is readily found that this reaction is basically concerted one, and no radical is created on the way. On the other hand, hydrogen atom migration is usually represented schematically as



Indeed, the spatial distribution and its number of thus created radical electrons are very clearly calculated in terms of the unpaired electron density [28]. Since the hydrogen atom radical H^\bullet is created, this reaction is realized only in high energy processes such as those involving states that are photoexcited.

To illustrate how the unpaired electrons are created and distributed in space on the way of the hydrogen migration in the excited state reaction (S_1 state) of



we show the distribution of $D(\mathbf{r})$ in Fig. 3(b), which is compared with panel (a) exhibiting a proton transfer reaction dynamics in the ground state counterpart, that is



It is clearly observed that a large distribution of $D(\mathbf{r})$, drawn in yellow lobes, covers the moving hydrogen atom nucleus, along with those generated also on oxygen and nitrogen atoms. In contrast, virtually no $D(\mathbf{r})$ is detected in the proton transfer (panel (a) in Fig. 3).

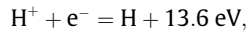
This example demonstrates also the utility of the unpaired electron density, which will be applied to our targeted reactions later.

2.3. Proton transfer in the ground states accompanied by backward electron flow

The second important characteristic of proton transfer of Eq. (6) is the way of charge redistribution anticipated in its dynamics. A naive question is whether the bare proton (H^+) is generated on the way in such a manner that



However, this seemingly rational (and common sense) process should be denied in the ground state dynamics, if one considers



which suffers huge endothermicity. Therefore there should be a physical trick behind the proton transfer dynamics.

The mechanism and its dynamics for the reaction of Eq. (6) to be possible has been clarified with use of the electron flux analysis [28]. The dynamical flow of electrons within a molecule can be directly monitored in terms of the probability current density $\mathbf{j}(\mathbf{r}, t)$ that satisfies the continuity equation

$$\frac{\partial \rho(\mathbf{r}, t)}{\partial t} + \nabla \cdot \mathbf{j}(\mathbf{r}, t) = 0. \quad (11)$$

In quantum mechanics $\mathbf{j}(\mathbf{r}, t)$ is defined as

$$\mathbf{j}(\mathbf{r}, t) = \frac{\hbar}{2im_e} [\psi^* \nabla \psi - \psi \nabla \psi^*], \quad (12)$$

which we simply call the Schiff flux [29], where m_e and ψ are the mass and wave function of the involved particles. For many-electron systems it is redefined as

$$\mathbf{j}(\mathbf{r}, t) = \frac{\hbar}{2im_e} [\nabla_{\mathbf{r}} \rho(\mathbf{r}', \mathbf{r}) - \nabla_{\mathbf{r}'} \rho(\mathbf{r}', \mathbf{r})] \Big|_{\mathbf{r}'=\mathbf{r}}, \quad (13)$$

where $\nabla_{\mathbf{r}}$ and $\nabla_{\mathbf{r}'}$ are the nabla with respect to \mathbf{r} and \mathbf{r}' , respectively. In Eq. (13) the coordinates \mathbf{r}' are to be replaced with \mathbf{r} after the derivative is done. As seen from Eq. (12), only complex-valued wave functions can give non-zero flux. Indeed, stationary-state electronic wavefunctions like most of the eigenfunctions of the electronic Hamiltonian $\hat{H}^{(el)}$ in quantum chemistry are real-valued, and thereby electron flux given by them are identically zero everywhere. (See Refs. [17,28,30–33] for applications of electron flux in chemical dynamics.) Incidentally, the present work treats only the electronic

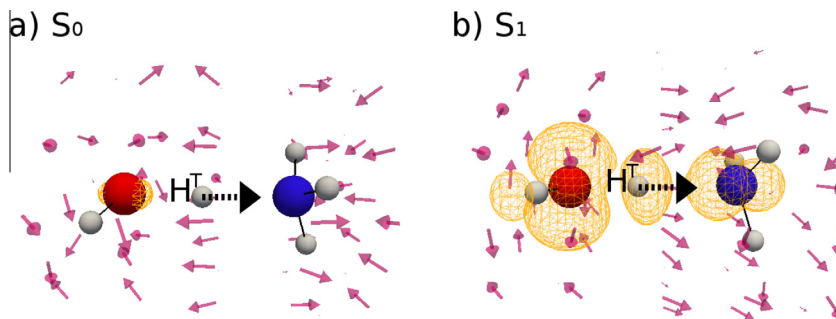


Fig. 3. Illustrative examples of (a) concerted proton transfer $\text{H}_2\text{O} + \text{NH}_3 \rightarrow \text{OH}^- + \text{NH}_4^+$, and (b) hydrogen atom migration $\text{H}_2\text{O} + \text{NH}_3 \rightarrow \text{OH}^- + \text{NH}_4^+$, which correspond to the ground-state (S_0) and the excited-state (S_1) dynamics, respectively. The transferred hydrogen nucleus is referred to as H^\ddagger with momentum indicated by the dashed arrow. The solid arrows denote the electron flux $\mathbf{j}(\mathbf{r})$, while the contour meshes in yellow correspond to the spatial distribution of the unpaired electron density $D(\mathbf{r})$. In the concerted proton transfer (a), virtually no unpaired electron is observed on H^\ddagger , and electron flux vectors in the vicinity of H^\ddagger point to the opposite direction of the motion of the H^\ddagger (from left to right). On the other hand, in the hydrogen atom migration (b), obviously has large components of unpaired electrons on O, H^\ddagger , and N atoms. Besides, the electron fluxes point to the same direction as the motion of H^\ddagger . H = gray, O = red, N = blue.

flux at each nuclear configuration. Manz and his group have been studying such total electronic and nuclear flux [31,32,34].

Fig. 3 for reactions in S_0 and S_1 of Eq. (8) depicts the electron flux vectors on the way of transfer of H^T . The electron flux generally fluctuates rather rapidly (much faster than the time scale of nuclear motions), but overall behavior clearly indicates the direction and amount of flow of electron within a molecular system. As panel (a) in this figure shows, electrons flow backward with respect to the motion of H^T . On the other hand, the electronic charge covering the moving H^T in panel (a) is kept almost constant throughout the proton transfer reaction. Thus the backward electron flux partly manifests electronic population being rendered back to the water side, which results in +1 charge transfer indicated as in Eq. (9).

Using the electron flux as above, we have found that the reaction of Eq. (6) proceeds as follows: In Eq. (10)



is generated, instead of $A^- + H^+$, in the manner of concerted reaction, where $H^{\Delta+}$ implies a proton nucleus tightly covered with 1s electrons as much as the population of $n = 0.4 – 0.7$ (depending on the systems under study), thus giving rise to $1 – n$ effective (positive) charge on the proton, which is represented as $H^{\Delta+}$. Then, the amount of electron as much as n is rendered back to A^Δ through different spatial channels [35]. This electron back-flow can be monitored directly with the electron flux described as above. Then after all A^- and H^+B are produced even in the low energy ground states. A theoretical consequence from this mechanism is that the dynamics of proton transfer can be affected (or even controlled) by modulating the pathways of electron back-flow with changing solvents and/or substituent effects.

2.4. Summary needed to proceed for coupled proton electron transfer

As for the ground state proton transfer: (1) It is a concerted reaction. (2) The transferring proton is never naked but tightly covered with a portion of the 1s electron cloud, the same amount of which electrons is rendered back to the original molecular site, and thereby accomplish the transfer of charge of one proton. (3) Charge separation is realized in the form of A^- and H^+B .

The excited state hydrogen migration reaction requires a mechanism to create hydrogen atom radical. The distribution of the radical can be monitored in terms of the unpaired electron density. The transferring hydrogen atom is usually produced by direct photoexcitation to dissociate chemical bonds such as C-H. Or an indirect way of producing hydrogen atom is clearly seen in $\pi - \pi^*$ excitation of the benzene-ring of phenol molecule. After somewhat a long time, hydrogen atom is ejected from -OH group, the energy of which is transmitted through the nonadiabatic transition that couples the $\pi - \pi^*$ state and $\sigma - \sigma^*$ state [14,15].

3. Photochemical mechanism of charge separation

We now scrutinize the excited-state mechanism of triggering the charge separation (proton-electron pair creation) dynamics of photoinduced water-splitting reaction ($2H_2O \rightarrow 4H^+ + 4e^- + O_2$) catalyzed by Mn-H₂O systems, highlighting the major difference of this mechanism from the very basic dynamics of proton transfer and hydrogen atom migration as summarized above. Our chosen model systems are generally expressed as X-Mn-OH₂··A, where X = (OH, Ca(OH)₃) and A = (N-methylformamide, guanidine, imidazole or ammonia cluster). We first show that electron transfer does not take place in the electronic ground state even if proton transfer happens to be realized, thus resulting in no charge separation. We then proceed to the dynamics of excited electronic states,

finding both an electron and a proton are simultaneously transferred to the acceptors through conical intersections. In this mechanism, the electron takes different pathways from that of the proton and reach the Rydberg-like states of the acceptors, thereby inducing charge separation in A. We find another crucial nonadiabatic process that deteriorates the efficiency of charge separation by rendering the created pair of proton and electron back to the originally donor site through the states of d-d band originated from Mn atom. We address this dynamics by means of a path-branching representation. The dynamical roles of a doped Ca atom are also revealed; change of the pathways of electron flow and reducing the annihilation dynamics of proton-electron pair.

3.1. Method of nonadiabatic electron dynamics

The theoretical method we here use is nonadiabatic electron wavepacket dynamics in the path-branching representation. Since it has been described rather extensively elsewhere [36–43], we outline only its framework. First, for the standard nonrelativistic full dimensional electronic and nuclear Hamiltonian

$$H(\mathbf{r}, \mathbf{R}) = \frac{1}{2} \sum_k \hat{P}_k^2 + \hat{H}^{(el)}(\mathbf{r}; \mathbf{R}). \quad (14)$$

$H^{(el)}(\mathbf{r}; \mathbf{R})$ is the so-called electronic Hamiltonian. We represent the electronic wavepackets that are to be propagated in time along nuclear paths $\mathbf{R}(t)$ as

$$\Psi_{elec}(\mathbf{r}, t; \mathbf{R}(t)) = \sum_I C_I(t) \Phi_I(\mathbf{r}; \mathbf{R}) \Big|_{\mathbf{R}=\mathbf{R}(t)}, \quad (15)$$

with \mathbf{r} and t being electronic and time coordinates, respectively. $\{\Phi_I(\mathbf{r}; \mathbf{R}(t))\}$ serves as a basis set. The time-dependent coefficients $C_I(t)$ are to be determined with respect to the basis functions. The motion of Ψ_{elec} is driven by the coupled equations

$$i\hbar \frac{\partial C_I}{\partial t} = \sum_J \left(H_{IJ}^{(el)} - i\hbar \sum_k \dot{R}_k X_{IJ}^k - \frac{\hbar^2}{4} \sum_k (Y_{IJ}^k + Y_{JI}^{k*}) \right) C_J, \quad (16)$$

where

$$H_{IJ}^{(el)} = \left\langle \Phi_I \left| \hat{H}^{(el)} \right| \Phi_J \right\rangle, \quad X_{IJ}^k = \left\langle \Phi_I \left| \frac{\partial}{\partial R_k} \right| \Phi_J \right\rangle \text{ and } Y_{IJ}^k = \left\langle \Phi_I \left| \frac{\partial^2}{\partial R_k^2} \right| \Phi_J \right\rangle, \quad (17)$$

with R_k being the k th component of \mathbf{R} . The second order terms Y_{IJ}^k are neglected in our usual practice, which should be justified by the presence of the factor \hbar^2 multiplied.

The set of coupled Eqs. (16) is essentially equivalent to

$$i\hbar \frac{\partial}{\partial t} \Psi_{elec}(\mathbf{r}, t; \mathbf{R}) \Big|_{\mathbf{R}=\mathbf{R}(t)} = \left(\hat{H}^{(el)} - i\hbar \sum_k \frac{dR_k}{dt} \frac{\partial}{\partial R_k} - \frac{\hbar^2}{4} \sum_k \frac{\partial^2}{\partial R_k^2} \right) \Psi_{elec}(\mathbf{r}, t; \mathbf{R}) \Big|_{\mathbf{R}=\mathbf{R}(t)}, \quad (18)$$

which may be rewritten in a form

$$\left(\frac{\partial}{\partial t} + \sum_k \frac{dR_k}{dt} \frac{\partial}{\partial R_k} \right) \Psi_{elec}(\mathbf{r}, t; \mathbf{R}) \Big|_{\mathbf{R}=\mathbf{R}(t)} = \frac{1}{i\hbar} \left(\hat{H}^{(el)} - \frac{\hbar^2}{4} \sum_k \frac{\partial^2}{\partial R_k^2} \right) \Psi_{elec}(\mathbf{r}, t; \mathbf{R}) \Big|_{\mathbf{R}=\mathbf{R}(t)}. \quad (19)$$

The time derivative operator in the left hand side

$$\frac{D}{Dt} = \frac{\partial}{\partial t} + \sum_k \frac{dR_k(t)}{dt} \frac{\partial}{\partial R_k} \quad (20)$$

is the so-called Lagrange derivative, which is frequently used in fluid mechanics to track the dynamics from a view point moving

along a flow line defined by the vector field of $\mathbf{R}(t)$. This time-derivative transforms Euler's view of fluid dynamics (viewed from a fixed coordinate system as in Eq. (16)) to the Lagrange view. A formal solution of Eq. (19) is given as

$$\Psi_{\text{elec}}(\mathbf{r}, t + \Delta t; \mathbf{R}(t + \Delta t)) = \exp \left[\frac{1}{i\hbar} \int_{t(\text{path})}^{t+\Delta t} \left(\hat{H}^{(\text{el})} - \frac{\hbar^2}{4} \sum_k \frac{\partial^2}{\partial R_k^2} \right) \right] \Psi_{\text{elec}}(\mathbf{r}, t; \mathbf{R}) \Big|_{\mathbf{R}=\mathbf{R}(t)}, \quad (21)$$

where $\int_{t(\text{path})}^{t+\Delta t}$ indicates an integral along a path given by $\mathbf{R}(t)$ for a short time. Thus Ψ_{elec} is carried along a path $\mathbf{R}(t)$ from a space-time point $(\mathbf{R}(t), t)$ to $(\mathbf{R}(t + \Delta t), t + \Delta t)$ with the quantum mechanical modulation as indicated in the right hand side of Eq. (21). This in turn represents rather explicitly how the electron flux is induced by the electron wavepacket dynamics.

As a basis set in Eq. (15), our standard practice is to use the so-called configuration state functions (CSF) or adiabatic electronic wavefunctions with a slight modification to avoid singular behavior at conical intersections. CSF basis are known to give a good quasi-diabatic representation, and moreover it generally enables stable computation for X_{ij}^k even in case of the passage of conical intersections. For any basis sets, we faithfully calculate both of $H_{ij}^{(\text{el})}$ and X_{ij}^k , which should minimize the effects due to different choices of basis sets. For the same reason both the avoided crossings (AX) and conical intersections (CI) can be treated in a unified manner without no computational distinction. Therefore we do not attribute or classify most of so many individual nonadiabatic transitions we are going to encounter to AX or CI. We refer such unidentified "couplings of the potential energy surfaces" to AX/CI. On the other hand, we will basically resort to the adiabatic representation in order to make physical interpretation about the computational results, no matter what kind of basis sets are chosen in practice. Hence we use the traditional term "nonadiabatic transition", even if the CSF (quasi-diabatic) basis are utilized in actual computations behind.

The nuclear path $\mathbf{R}(t)$ is driven by the so-called force matrix [36]

$$F_{ij}^k = - \left[\frac{\partial H_{ij}^{(\text{el})}}{\partial R_k} + \sum_K \left(X_{ik}^k H_{kj}^{(\text{el})} - H_{ik}^{(\text{el})} X_{kj}^k \right) \right] + i\hbar \sum_l \dot{R}_l \left[\frac{\partial X_{ij}^l}{\partial R_k} - \frac{\partial X_{ij}^k}{\partial R_l} \right], \quad (22)$$

which is equivalent to

$$F_{ij}^k = \left\langle \Phi_i \left| \frac{\partial \hat{H}^{(\text{el})}}{\partial R_k} \right| \Phi_j \right\rangle \quad (23)$$

only when the basis set $\{\Phi_l(\mathbf{r}; \mathbf{R}(t))\}$ was complete. For a finite basis set, approximate use of the Hellmann–Feynman type expression, Eq. (23), tends to give less accurate values. Because F_{ij}^k is a matrix, it provides as many forces to nuclei as the number of involved electronic states at every small time step to induce infinite path-branching [37].

Technically it is impossible to obtain the exact solutions, which should be represented in terms of an infinite number of branching paths. Instead, we approximately generate a small number of representative paths to substitute a cascade consisting of the infinitely many branching paths [37]. Another more drastic approximation is to take an average of the force matrix over an electron wavepacket under study in such a way that

$$F_{\text{SET}}^k = - \sum_{IJ} C_I^*(t) F_{IJ}^k C_J(t) = - \left\langle \Psi_{\text{elec}}(\mathbf{R}(t)) \left| \frac{\partial \hat{H}^{(\text{el})}}{\partial R_k} \right| \Psi_{\text{elec}}(\mathbf{R}(t)) \right\rangle_{\mathbf{r}}, \quad (24)$$

which gives an averaged path rather than branching paths. The method using this averaged force coupled with the electronic wavepacket dynamics of Eq. (16) (without the terms of $-\frac{\hbar^2}{4} \sum_k (Y_{ij}^k + Y_{ji}^{k*})$) is called the semiclassical Ehrenfest theory (SET) [29]. SET gives accurate transition amplitudes and associated phases for a single passage of a nonadiabatic region, but the resultant paths cannot represent the branching situation at all. A good combination of the averaged paths and branching paths often provides an accurate yet computationally tractable compromise [37]. Indeed, we need a path-branching procedure later in this paper to study the successive passage of two conical interactions.

The equations of full-dimensional motion Eqs. (16) and (22) or (24) are numerically integrated in the on-the-fly scheme. Nonadiabatic systems like ones we are going to study demand much computational time. To carry out them in a practical time scale, we need a parallel algorithm for the computations of matrix elements such as $\partial H_{ij}^{(\text{el})} / \partial R_k$ and X_{ij}^k . (See [Supplementary material](#)).

3.2. Quantum chemical calculations

3.2.1. Static electronic structures

We employ the CISD/RHF level of calculation to describe the nonadiabatic electron wavepacket dynamics. Quantum chemical calculations are performed by using GAMESS programming package [44,45]. The atomic basis set is chosen to be Stevens, Basch, Krauss, Jasien, Cundari effective core potentials (SBKJC ECPs) [46] for Mn, Pople's 6-31G for (Ca, O, and C), and 6-31++G for (N, H). Recall that 6-31++G basis set includes diffuse functions, which are crucial to describe the present mechanism [17,26]. The CISD active space is chosen to be HOMO–(HOMO + 80) to obtain the configuration state functions (CSFs), the total number of which amounts to 3321. This level of calculation has been carefully chosen to be a good compromise between quality and computational cost (see [Supplementary material](#)). Note that each computation of a single representative path calls thousands of quantum chemical calculations in total, and the computational cost nonlinearly increases as the size of basis set and/or the size of CISD active space. Prior to the full dynamics calculations, we performed RHF-level calculations for geometry optimization, vibrational analysis, and path sampling in the ground state. Those preliminary calculations dramatically reduce the computational cost without qualitative difference, since the adiabatic ground state is dominated by the RHF ground state all the way.

3.2.2. Characteristics of the critical molecular orbitals

Before performing nonadiabatic electron wavepacket dynamics, we need to survey the static properties of the systems. In particular the information of the LUMO is crucial for the present study. Fig. 4 displays the three-dimensional surface-representation of HOMO-2 to LUMO + 2, for X = OH in panel (a) and X = Ca(OH)₃ in (b) at the optimized geometries, as well as the energy levels of the MOs. Common frontier molecular orbitals (MOs) are found in the systems with X = OH and Ca(OH)₃, since the HOMOs are dominated by the Mn d-shell and LUMO is by the Rydberg-like states. As shown in the previous studies, these Rydberg-like diffused states are critically important as an electron accepting machinery.

The HOMOs are well isolated in energy from the HOMO-1, which allows us to exclude the CSFs of excitation from those lower MOs (see [Supplementary material](#)). On the other hand, the energy levels of the virtual orbitals are much denser.

The HOMO–LUMO gap is calculated to be approximately 5 eV. This gap does not give the photoexcitation energy, and indeed the configuration interaction calculations actually give 3.0–3.5 eV to the lowest photoexcitation energy. In fact, the very small value of the oscillator strength between the ground and n th excited state

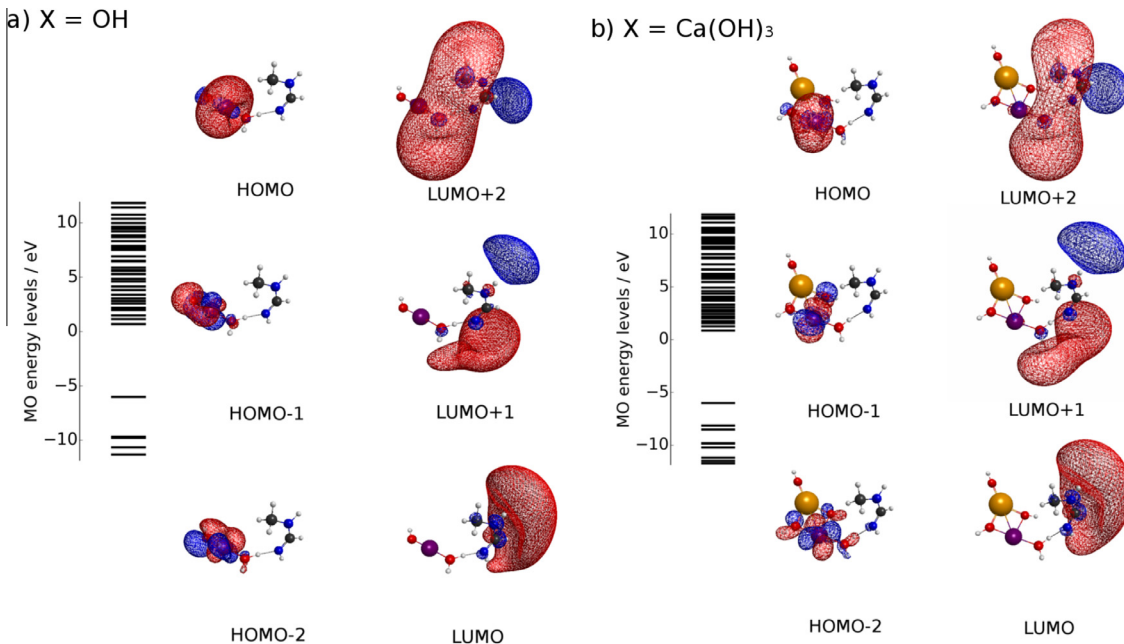


Fig. 4. Spatial distribution of the frontier MOs ((HOMO-2)–(LUMO + 2)) and their peripheral energy levels. Those of $X = \text{OH}$ and $X = \text{Ca}(\text{OH})_3$ are quite similar to each other in the way that HOMO is dominated by the Mn d-shell, and LUMO is by the Rydberg-like diffused states of the acceptor. Mn = purple, Ca = orange, O = red, N = blue, C = black, and H = gray.

f_{on} precludes the HOMO–LUMO photoexcitation, the photochemical significance of which will be discussed later. The photoexcited states at the beginning are expressed in terms of many CSFs of excitation to MOs higher than or equal to LUMO + 2. This is a reason why we need to take such a large number of virtual MOs into account.

Interestingly, the model system of $X = \text{Ca}(\text{OH})_3$, including a Ca atom, HOMO–(LUMO + 2) are seen to be topologically very similar to the corresponding MOs of $X = \text{OH}$ as comparison between panel (a) and (b) in Fig. 4 shows, which suggests that Ca might not have significant influence on the chemical property in this level. However, this is not the case, as will be discussed later.

3.3. Ground-state dynamics: no electron transfer occurs

We begin our electron dynamics with a survey of the ground state dynamics. In many text books of biological chemistry it is described that water splitting in PSII system takes place with the help of a catalytic action by the Mn cluster that assists electrons and protons to be pulled away from the system in ground state. No perfect explanation about this mechanism has been given to the best of our knowledge. It is well established that there are some other antenna molecular systems responsible for photon absorption. However, this fact alone does not warrant that the series of reactions in PSII system proceed without photoexcitation energy. Although the present paper is not concerned with natural photosynthesis, we should herein examine whether or not the charge separation (electron–proton pair creation) can indeed happen in the ground state of our systems.

3.3.1. Dynamics of zero-point vibrational energy

To start the nuclear dynamics, we assign the zero point (vibrational) energy ($0.5 \hbar \omega$) to each normal mode. Since the ground state is dominated by the RHF ground state configuration, we just run *ab initio* molecular dynamics with the RHF level of calculation to approximately obtain the path of zero-point vibration

with the CISD/RHF level. It saves much computational cost but should bring about qualitatively the same results. The sample points for excited-state dynamics are randomly picked up from this path. Thirty and five sampling points are chosen for $X = \text{OH}$ and $X = \text{Ca}(\text{OH})_3$, respectively.

Here we focus on the motion of H^{T} along the path of zero-point vibration (see Fig. 1 for the definition of H^{T}). The other hydrogen atoms are nonreactive. Time variation of the internuclear distances OH^{T} (R_{OH}) and NH^{T} (R_{NH}) of the $\text{O}-\text{H}^{\text{T}} \cdots \text{N}$ bonds is shown in Fig. 5. We see that R_{OH} of both $X = \text{OH}$ and $\text{Ca}(\text{OH})_3$ are kept as long as ca. 1.0 Å, while R_{NH} ranges from 1.4 to 2.2 Å, which is a little more fluctuating because of the weak hydrogen bonding. These results claim clearly that no proton transfer takes place in the ground state easily in contrast to the excited state. We illustrate explicitly how the H^{T} transfer looks like in photoexcited dynamics in Section 3.4.

3.3.2. Electron population analysis

To survey whether or not electrons are carried over from Mn side to the other side, we perform a “regional population analysis” by summing up the atomic population at each region predefined inside the super-molecule. We here use the term “regional” to distinguish the submolecular parts of the entire target system, namely, an electron–proton donor (EPD), H^{T} , and an electron–proton acceptor (EPA). EPD consists of $\text{X}-\text{Mn}-\text{OH}$, while EPA is the electron–proton acceptor itself, which has been referred to as A so far.

To identify whether radical electrons are created (as in an isolated hydrogen atom), we consider the total electron density $|\Psi_{\text{elec}}(\mathbf{r})|^2$ and the unpaired electron density $D(\mathbf{r})$ defined in Eq. (3). In practice, the regional population analysis is performed as follows. First we assign $D(\mathbf{r})$ to the atoms by means of Löwdin's method to obtain atomic population [47] in stead of Mulliken's original method [48], since it is known that a naive application of the latter often leads to less appropriate interpretation when the Rydberg-like diffused orbitals are involved. We then sum up the atomic population at each region (EPD, H^{T} , and EPA). The resulting

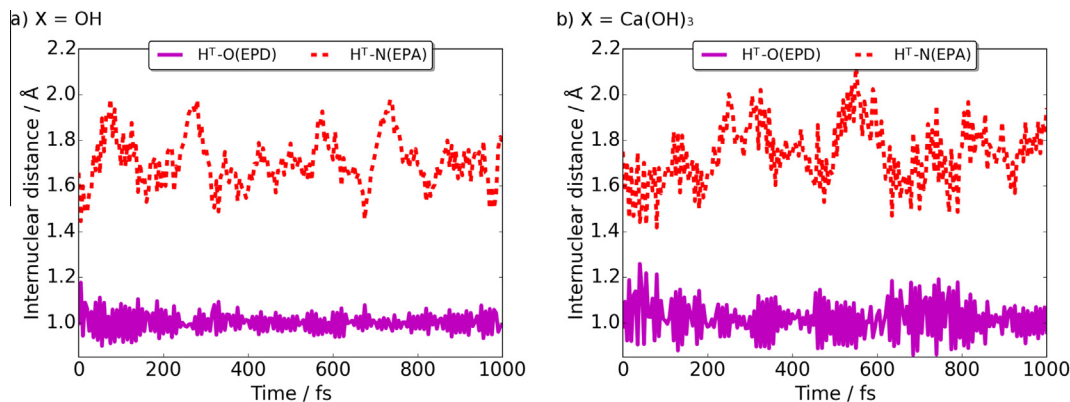


Fig. 5. Time variation of R_{OH} (solid line) and R_{NH} (dashed line) along a path of the zero point oscillation on the ground electronic state. The H^{T} transfer is not observed for both $X = \text{OH}$ and $\text{Ca}(\text{OH})_3$.

regional populations are referred to as regional electron population P_M and regional unpaired electron population D_M , in which M denotes the part of the system, that is, EPD, H^{T} , and EPA. We use regional charge $Q_M = Z_M - P_M$ instead of P_M for the sake of convenience, in which Z_M is the sum of nuclear charges of each part.

Time variation of Q_M and D_M along the ground-state paths are shown in Fig. 6. It is seen that Q_M on EPA is kept neutral, while those on H^{T} and EPD are +0.4 and -0.4, respectively. On the other hand D_M on EPA and H^{T} are virtually zero, while that of EPD is kept as much as 0.5. This amount of the total unpaired electrons usually arises from electron correlation mainly due to the double excitation electronic configurations in the 3d-orbital space of Mn atom, which has nothing direct to do with molecular interaction with EPA. Therefore, it is obvious that no significant changes in both Q_M and D_M have happened in the ground state. This should be consistent with the fact that neither proton transfer nor hydrogen atom migration takes place. These data should be compared later with the photoexcited dynamics.

The presence of the Ca atom does not make any significant differences in the ground state. The regional charge and the regional unpaired electron population of $X = \text{Ca}(\text{OH})_3$ are qualitatively the same as those of $X = \text{OH}$, as we have seen in MOs (Fig. 4). Therefore, adding $\text{Ca}(\text{OH})_2$ to the $X = \text{OH}$ system does not suggest significant effect as far as the ground-state dynamics is concerned.

3.4. Photoexcited dynamics of coupled proton-electron transfer (CPET)

3.4.1. Nuclear paths after vertical excitation from those running on the ground-state

Now we proceed to the photoexcited-state dynamics, where both an electron and a proton are transferred from EPD to EPA in a collective manner. To prepare the initial conditions for nuclear paths, we randomly selected phase space points from the ground-state paths, and lifted the electron wavepacket on each sample point up in the photoexcited state. An electronic wavepacket state has been prepared with equal weights (with no bias), picked up from among those adiabatic states that lie in the range of excitation energy of 3.0–3.5 eV and have oscillator strengths f_{0n} larger than 0.1. One can choose other sets of the weights in the superposition to maximize the production rate of the electron-proton pair, but our preliminary study shows that the qualitative aspect presented below in the present coupled proton-electron transfer dynamics does not basically depend on the ratio of state-mixing, since the excited states involved herein are more or less similar to each other. Thus the phenomena turn out to be robust.

In all the systems thus excited, both H^{T} and an electron are transferred from EPD to EPA, with different speed along their own pathways. The transfer of H^{T} is associated with nonadiabatic transition, through which unpaired electrons transfer to the Rydberg-like state of EPA. This makes a marked difference from the ground-state dynamics. Since it has turned out in our preliminary survey [26] that the basic mechanism of CPET underlying all the dynamics we studied are qualitatively the same, we pick in what follows only one among them, as those in Fig. 1, to demonstrate the mechanism. In doing so we first describe the results of $X = \text{OH}$, and then briefly mention to the case of $X = \text{Ca}(\text{OH})_3$.

3.4.2. Photoexcited H^{T} transfer

As can be tracked in Fig. 7, H^{T} transfer induced by photoexcitation occurs within a scale of ~100 fs. Recall that the H^{T} transfer did not take place even in 1000 fs in the ground state. A rather precise dynamics reflected in R_{OH} and R_{NH} along a path is seen in Fig. 7(a), which should be compared with Fig. 5(a) for the ground state. In this path, H^{T} transfer occurs at $t = 49$ fs and it does not return shortly. The concomitant nonadiabatic transition along the H^{T} transfer can be observed in Fig. 8(a), in which the potential energy gaps between the excited states and the ground electronic state at nuclear configuration $\mathbf{R}(t)$, that is $V_n(\mathbf{R}(t)) - V_0(\mathbf{R}(t))$ ($n = 1, 2, \dots$), are graphed, where $V_n(\mathbf{R}(t))$ is the adiabatic electronic energy of the n th state at $\mathbf{R}(t)$. Blue cloud-like shadow superimposed over the curves in this figure represents the population occupied by the states; the darker is the shadow, the larger is the population. It is clearly seen in these graphs that around 50 fs $V_n(\mathbf{R}(t)) - V_0(\mathbf{R}(t))$ of the adiabatic states constituting the wavepacket quickly become smaller (the relevant $V_n(\mathbf{R}(t))$ come close to the ground state energy) after passing through a complicated looking valley area, which are formed by the state committing to strong nonadiabatic couplings. Fig. 8(a) indicates that at a later time, around $t = 80$ fs, after the major nonadiabatic transition, two adiabatic states seem to be dominantly occupied by the total electron wavepacket. In particular, the lowest curve, which is asymptotically connected back to the d-d state of Mn, is seen to newly start to be occupied around the time $t = 60$ fs. We will come back to this aspect later in a great detail.

Meanwhile we scrutinize how the associated electron dynamics takes place along with the H^{T} transfer. We first survey the dynamics of unpaired electrons. Some selected snapshots of the spatial distribution of unpaired electrons $D(\mathbf{r})$ are shown in Fig. 9(a). At $t = 47.5$ fs, which is just before the H^{T} transfer, the major part of the unpaired electron density lies mostly on the EPD side as a localized biradical pair. And then a part of them is transferred to the Rydberg-like state of EPA, resulting in an asymptotic

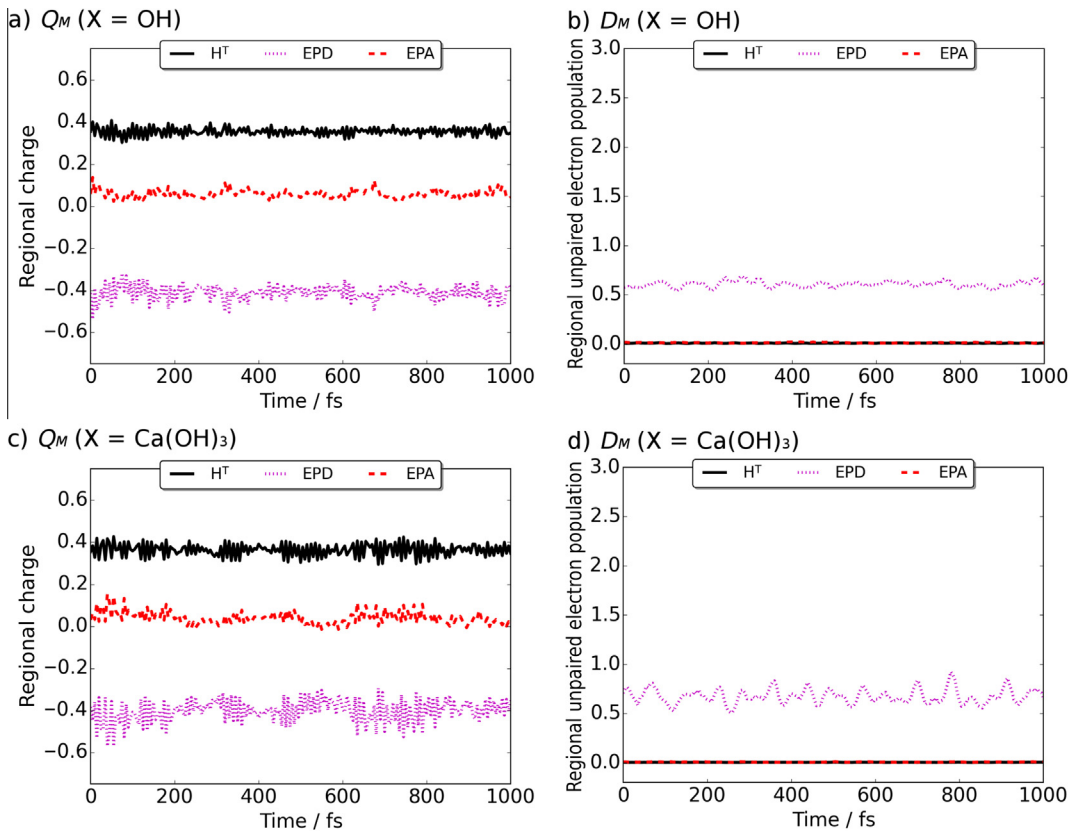


Fig. 6. Time variation of the regional charge Q_M and the regional unpaired electron population D_M along the same path as that in Fig. 5 for $X = \text{OH}$ and $\text{Ca}(\text{OH})_3$.

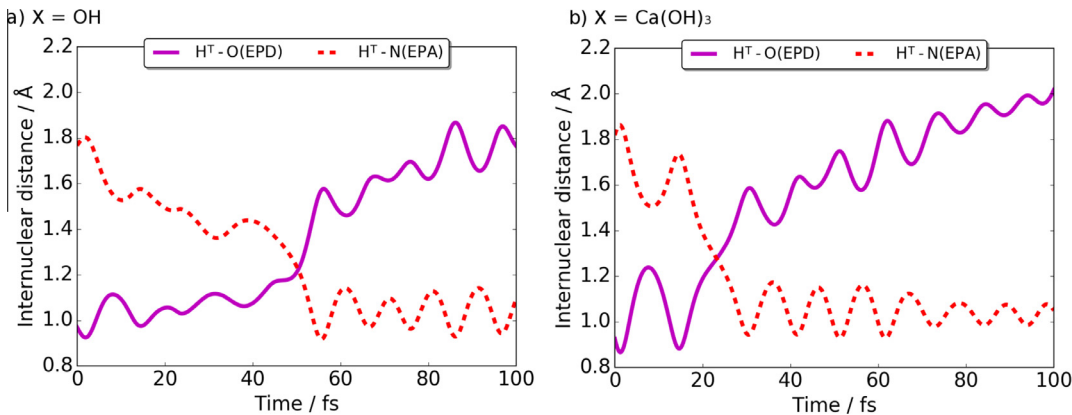


Fig. 7. Time variation of R_{OH} (solid line) and R_{NH} (dashed line) along one of the photoexcited-state paths relevant to CPET. In both $X = \text{OH}$ and $X = \text{Ca}(\text{OH})_3$, the graphs of R_{OH} and R_{NH} cross each other, which represents the H^T transfer.

(well separated) biradical. Notice that the unpaired electrons take their own pathways different from that of the nucleus of H^T . That is, while the proton is linearly shifted, the electrons move circularly as though they are captured by the Rydberg-like diffused states. These collective dynamics along different paths are the dynamical identification of the present coupled proton-electron transfer (CPET).

The arrows in Fig. 9(a) correspond to the Schiff probability current density (or flux, in short) [29] for electrons. The electron-flux studies on chemical reactions have been made by Takatsuka and coworkers [30,28,33,39,17], and Manz and coworkers [31,32,34], which have proven to be useful to track the detailed electronic pathways. The flux shown in the snapshot at $t = 49.0$ fs in Fig. 9

(a) clearly illustrates the semi-circular motion of electrons pointing to the Rydberg-like states, in contrast to the linear motion of the nucleus of H^T .

3.4.3. Population analysis on CPET; hydrogen atom migration?

Thus CPET turns out to consist of H^T transfer and electron flow passing through mutually different paths. We further characterize the electronic states of H^T in CPET by closely looking at the regional charge Q_M (Fig. 10(a)) and the regional unpaired electron population D_M (Fig. 10(b)) as we did for the ground state. Q_M on H^T is kept approximately +0.4, which is similar to that of the ground state (Fig. 6(a)). Besides, the regional unpaired electron population D_M on H^T is kept virtually zero, which is also the same in the ground

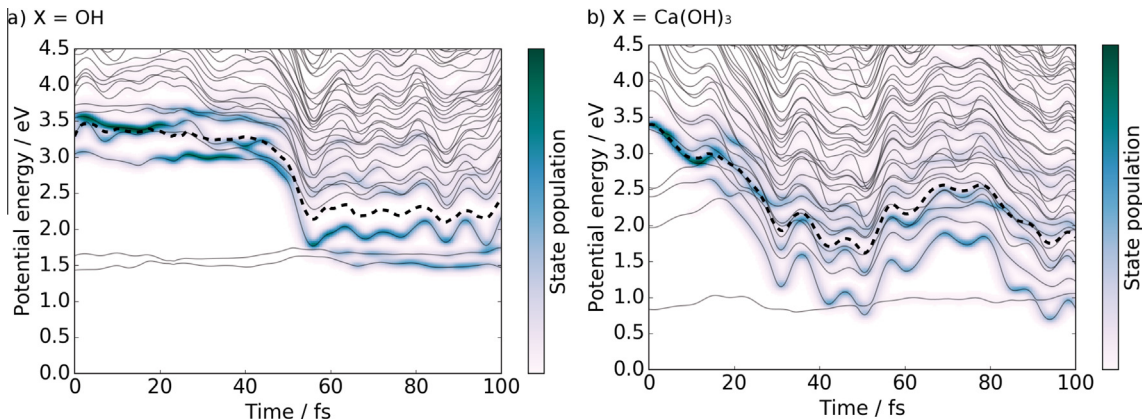


Fig. 8. The potential energy gaps $V_n(\mathbf{R}(t)) - V_0(\mathbf{R}(t))$ (solid line) along one of the photoexcited-state paths undergoing CPET. The dashed line represents the mean electronic energy of the wavepacket state. The cloud-like shadow over the energy-gap curves represents the state population of the relevant adiabatic states. The darker color indicates the larger population. The electronic states of almost constant values of $V_n - V_0$ around 1.5 eV ($X = \text{OH}$) and 0.8 eV ($X = \text{Ca}(\text{OH})_3$) are the d-d states.

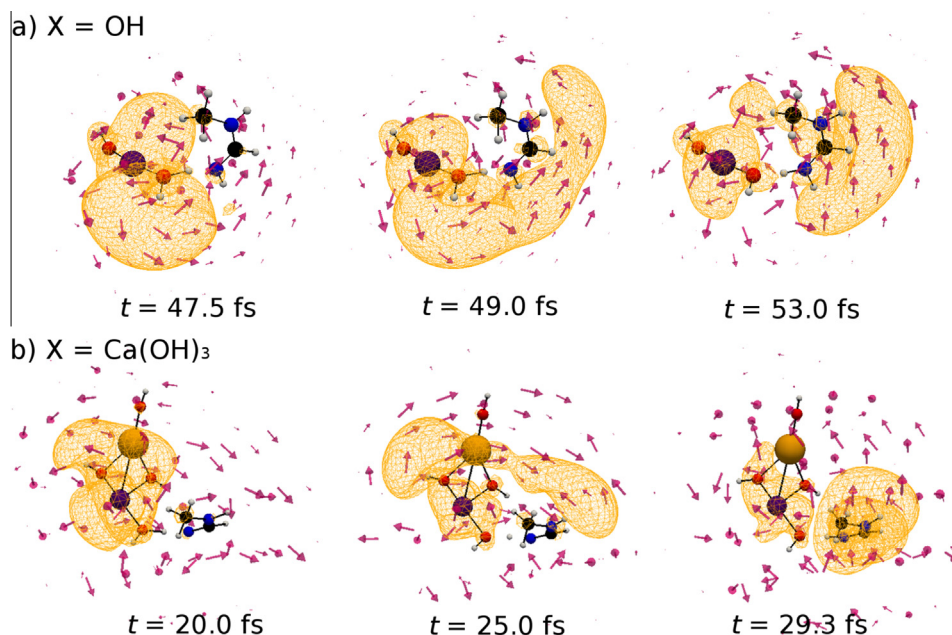


Fig. 9. Selected snapshots of the spatial distribution of the unpaired electron density $D(\mathbf{r})$ along one of the photoexcited-state paths relevant to CPET. The arrows indicate the electron flow (flux) induced by nonadiabatic transitions. Large values coming from the inner shell electrons have been neglected for clearer visualization.

state (Fig. 6(b)). Therefore it turns out that as far as the transfer of H^{T} alone is concerned, it is like a concerted reaction just like the transfer of H^{T} in the ground state.

It is important to distinguish CPET from H radical transfer, or H atom migration. They are similar to each other in that both an electron and a proton are transferred from EPD to EPA. However, the H radical transfer alone does not directly induce charge separation. Besides, an energy as high as 13 eV is required to make a complete separated pair of proton and electron from a hydrogen atom. Therefore creation of the proton-electron pair should be achieved in a different manner. If hydrogen atom migration actually takes place in the present H^{T} transfer system, newly formed NH bond should break the double bond to a single one in N-methylformamidine (see Fig. 1), leaving a new radical center behind on the central C atom. However, such a to-be-born radical is not seen in Fig. 9(a), except for a very minor component. More clearly and directly, if radical is created on H^{T} Q_M and D_M of H^{T} should be virtually zero and unity, respectively, as described in Section 2. But this is certainly not the case, as readily confirmed in Fig. 10(a).

3.5. Backward transfer of H^{T} and electron via d-d states

Charge recombination after the charge separation is one of the most crucial processes that should be avoided to design efficient solar cells. In the present system to create a pair of electron and proton, such recombination can take place through another AX/CI following CPET, which leads the relevant excited electronic excited states down to the ground state of the acceptor molecule (EPA) [14,15]. This type of recombination can be well avoided by successive proton relay and/or electron shift carrying them to mutually separated regions. We here find another physical process that may annihilate the pair of electron and proton created by CPET through a transition to the states of d-d band, which carry both H^{T} and electron back to the originally donor side (EPD) in the excited states but not to the ground state.

3.5.1. Tracking the second nonadiabatic transition after the CPET

Let us look back at Fig. 8(a), in which the dynamics of electronic state components of the wavepacket is traced by tracking the

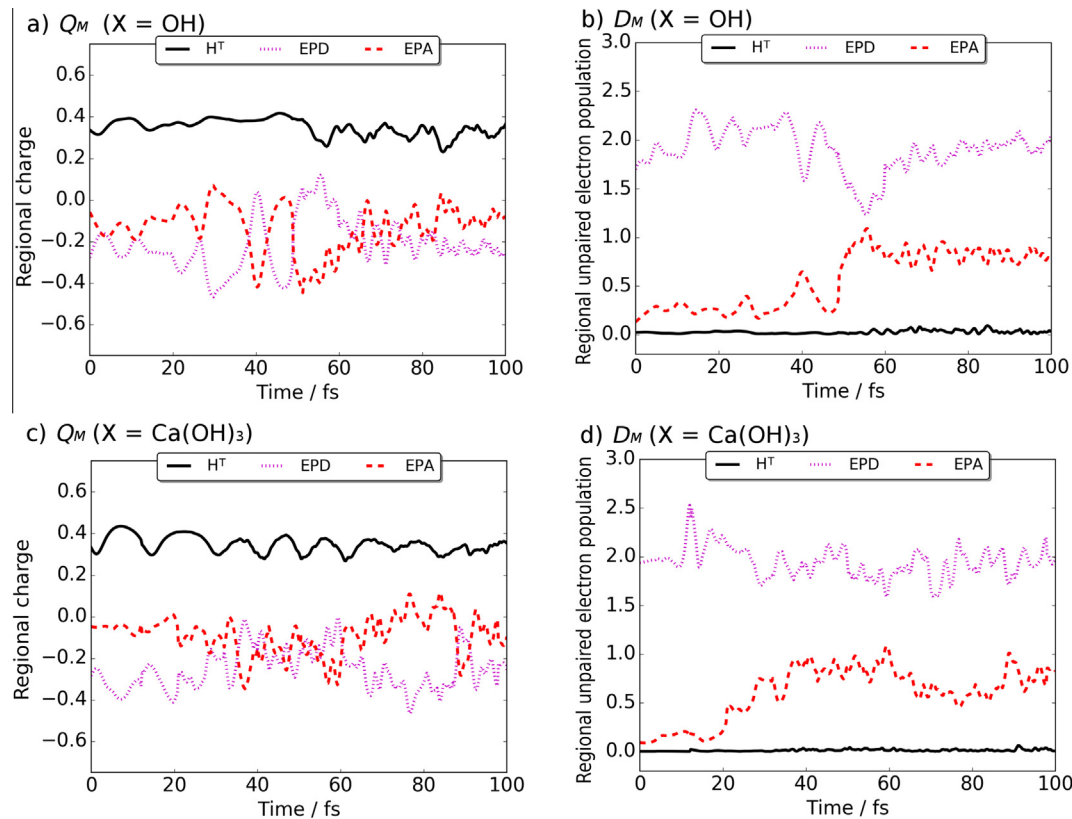


Fig. 10. Time variation of the regional charge Q_M and the regional unpaired electron population D_M along one of the photoexcited-state paths. Q_M and D_M on H^T are almost the same as those of the ground state (see Fig. 6). This means that the proton transfer in CPET is locally akin to the concerted proton transfer in the ground state, and only the manner of electron transfer is different.

adiabatic electronic-state energy curves ($V_n(\mathbf{R}(t)) - V_0(\mathbf{R}(t))$, $n = 1, 2, \dots$). The curves having the darker cloud-like shadow are of larger population in the expansion of Eq. (15). In this figure, the first nonadiabatic transition is observed at about $t = 49$ fs. Then all of sudden at around $t = 60$ fs, the two bottom curves, which represent the lowest two states originated from the d-d manifold of Mn atom, have become populated. Closer examination shows that these two curves undergo nonadiabatic couplings at the right-side wall of the region (d) in Fig. 2 (not depicted there). Thus only after about 10 fs of the first and major nonadiabatic transition (around $t = 49$ fs), the wavepacket encounters the second one, by which a considerably large portion of the electronic wavepacket is guided to the d-d band states.

The electronic properties of these d-d states are quite different from the other major parts of the state that have carried the H^T and electron as CPET. Among others, it is intuitively captured by an inspection over Fig. 8(a) that the forces (which is actually proportional to the derivative of the potential curves) arising from the d-d band adiabatic potential surfaces are qualitatively different from the others. Therefore in order to faithfully track what happens after the second nonadiabatic coupling, we give up the SET there and resume to track the successive dynamics with path-branching representation.

3.5.2. Path-branching to the groups of states

The general algorithm of natural and smooth path-branching has been formulated and implemented in our path-branching code with the force matrix [36,37,39,41–43]. However, this

algorithm is intended to cope with nonadiabatic transitions for rather simple cases where a few potential surfaces nonadiabatically couple with one another. In contrast, the system we here treat contains the Rydberg-like quasi-degenerate states, and moreover there are qualitatively only two channels to be branched at this second transition. Therefore we generalize the notion of path-branching so that paths are branched to the group of states; one is the d-d state group and the other is the major group consisting of the Rydberg-like states forming the region (d) in Fig. 2. Such a pair of branched paths are exemplified in Fig. 11.

As a conventional way of path-branching for the quasi-degenerate state, we take the following approach: Suppose that at time $t = \tau$ the electron wavepacket begins to be partitioned into two parts, each of which is composed of a set (group) of adiabatic states such that

$$\begin{aligned} \Psi_{\text{elec}}(\mathbf{r}, \tau; \mathbf{R}(\tau)) &= \Psi_{\text{elec}}^{(1)}(\mathbf{r}, \tau; \mathbf{R}(\tau)) + \Psi_{\text{elec}}^{(2)}(\mathbf{r}, \tau; \mathbf{R}(\tau)) \\ &= \sum_{m(\text{adiabatic})}^{\text{Group}\#1} C_m^{(1)}(\tau) \Phi_m^{(1)}(\mathbf{r}; \mathbf{R}(\tau)) + \sum_{n(\text{adiabatic})}^{\text{Group}\#2} C_n^{(2)}(\tau) \Phi_n^{(2)}(\mathbf{r}; \mathbf{R}(\tau)). \end{aligned} \quad (25)$$

Let $\mathbf{P}(\tau)$ be the momentum of the SET path at the position-time $\mathbf{R}(\tau)$. We resume a branching dynamics at this phase-space point $(\mathbf{R}(\tau), \mathbf{P}(\tau))$. At a later time $t = \tau + s$ ($s \geq 0$), by applying the following forces $F^{(1)k}(\tau + s)$ and $F^{(2)k}(\tau + s)$ on $\Psi_{\text{elec}}^{(1)}(\mathbf{r}; \mathbf{R}(\tau + s))$ and $\Psi_{\text{elec}}^{(2)}(\mathbf{r}; \mathbf{R}(\tau + s))$, respectively, which are defined as

$$\begin{cases} F^{(1)k}(\tau + s) = -\left\langle \Psi_{\text{elec}}^{(1)}(\mathbf{R}(\tau + s)) \left| \frac{\partial H^{(el)}}{\partial R_k} \right| \Psi_{\text{elec}}^{(1)}(\mathbf{R}(\tau + s)) \right\rangle / \left\langle \Psi_{\text{elec}}^{(1)}(\mathbf{R}(\tau + s)) \left| \Psi_{\text{elec}}^{(1)}(\mathbf{R}(\tau + s)) \right. \right\rangle \\ F^{(2)k}(\tau + s) = -\left\langle \Psi_{\text{elec}}^{(2)}(\mathbf{R}(\tau + s)) \left| \frac{\partial H^{(el)}}{\partial R_k} \right| \Psi_{\text{elec}}^{(2)}(\mathbf{R}(\tau + s)) \right\rangle / \left\langle \Psi_{\text{elec}}^{(2)}(\mathbf{R}(\tau + s)) \left| \Psi_{\text{elec}}^{(2)}(\mathbf{R}(\tau + s)) \right. \right\rangle \end{cases} \quad (26)$$

With these individually averaged forces, the two wavepackets are propagated in time in the form

$$\begin{cases} \Psi_{\text{elec}}^{(1)}(\mathbf{r}, \tau + s; \mathbf{R}_1(\tau + s)) = \sum_m^{\text{Group}\#1} C_m^{(1)}(\tau + s) \Phi_m^{(1)}(\mathbf{r}; \mathbf{R}_1(\tau + s)) \\ \Psi_{\text{elec}}^{(2)}(\mathbf{r}, \tau + s; \mathbf{R}_2(\tau + s)) = \sum_n^{\text{Group}\#2} C_n^{(2)}(\tau + s) \Phi_n^{(2)}(\mathbf{r}; \mathbf{R}_2(\tau + s)). \end{cases} \quad (27)$$

In this simplified approach, the off-diagonal elements of the force matrix have been neglected.

The next task is to appropriately make the groups $\Psi_{\text{elec}}^{(1)}(\mathbf{r}; \mathbf{R}(\tau))$ and $\Psi_{\text{elec}}^{(2)}(\mathbf{r}; \mathbf{R}(\tau))$. In the case studied in Fig. 8(a), we set the branching time τ at $t = 60$ fs (at the time of the second nonadiabatic transition). For $X = \text{OH}$, we can readily classify the adiabatic states into two groups; Group 1 contains those of the Rydberg-like diffused states, which accept much of the unpaired electrons after the first passage of the conical intersection around $t = 49$ fs. The d-d band states become populated only after the second nonadiabatic transition around $t = 60$ fs.

3.5.3. A channel of backward-transfers of proton and electron

We now track the fate of the states of the individual groups. We have calculated five pairs of such branching paths in total for $X = \text{OH}$. The path-branching is generally invoked during $t = 60\text{--}67$ fs. In this interval, the group populations are relatively stationary. We here pick a result in which the path-branching takes place at $t = 65$ fs.

An inspection over Fig. 11 clearly shows that the path of Group 2 after branching proceeds back to the EAD (originally donor) side. Since the electron wavepacket forming Group 2 consists of the d-d band states asymptotically connected to EPD site, the proton is rendered back to it on these potential surfaces of the d-d states. On the other hand, the path representing Group 1 undergoes

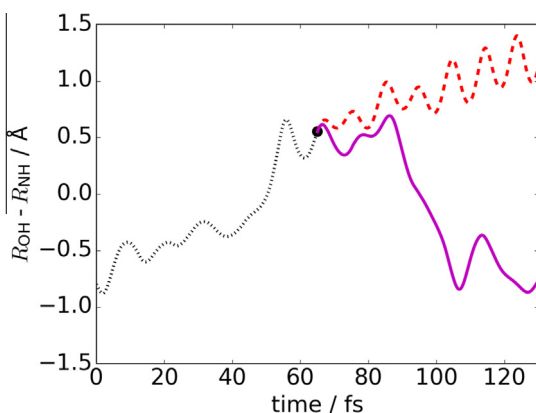


Fig. 11. Time variation of $R_{\text{OH}} - R_{\text{NH}}$ along a SET path (black dotted line) up to $t = 65$ fs, and then branching into two pieces responsible for Group 1 (red dashed line) and Group 2 (purple solid line) for $X = \text{OH}$. The path-branching is invoked at $t = 65$ fs. The path of Group 2 is seen to come back after all to the EPD site after branching.

vibrational motion in the EPA side (acceptor site), thus retaining both the transferred proton and electron as they are.

The spatial distribution of unpaired electron density along the paths of the two groups highlights the difference (see Fig. 12). The unpaired electron density along the path of Group 2 is seen to come back to EPD soon after the path-branching at $t = 65$ fs, and it does not change even at $t = 130$ fs. On the other hand, those of Group 1 is obviously the separated biradical state; one radical on EPD and the other in the Rydberg-like states of EPA. This character is still kept at $t = 130$ fs.

We further try to characterize the newly born branched paths. We first show (a) R_{OH} and R_{NH} , (b) $V_n(\mathbf{R}(t)) - V_0(\mathbf{R}(t))$ and state population, (c) Q_M , and (d) D_M for the path of Group 1 in Fig. 13 and that of Group 2 in Fig. 14. The representative path of Group 1 is similar to the parent SET path before branching, because this group made the major contribution to it. Fig. 13(b) shows that the wavepackets assigned as members of Group 1 undergo further nonadiabatic transitions to the d-d states successively, which should result that some more unpaired electrons on the Rydberg-like state of EPA is transferred back to EPD (see Fig. 12). In this recursive manner, the population of the pair of proton and electron once created by photoexcitation should be gradually reduced.

The properties along the representative path of Group 2 are considerably similar to those of the ground state. The electron wavepacket is dominated by the dark d-d states, namely, S_1 and S_2 (see Fig. 14(b)). These adiabatic states should provide similar dynamics to the ground state, since they run almost parallel to S_0 . According to Q_M (Fig. 14(c)), the H^T back-transfer is identified to be the concerted proton (back) transfer [35]. As for D_M (Fig. 14(d)) two radicals (unpaired electrons) survive throughout the process. Thus both the proton and unpaired electron have rendered back to the original site (EPD), not on to the ground state this time but to electronic excited states of the d-d band arising from Mn atom. The states on the d-d state will be eventually deactivated to the ground state with fluorescence, or may undergo other radiationless transitions, which are not identified in this study. We do not further track the possible deactivation processes in this work.

In summary we have found a chemical process in which the efficiency of photoexcited creation of a pair of proton and electron due to CPET is deteriorated. The mechanism of this new process is different from rather well-known mechanism of charge recombination as found in phenol plus ammonia clusters, in which the proton and electron recombine mutually in the place of EPD and the state is generally reduced to the ground state in a radiationless process through passing AX/Cl (see [14,28] for instance). Therefore the design of efficient catalysts for photo production of a pair of proton and electron demands a special care to prevent or close the channels of the backward transfer as well as the other charge recombination processes.

3.6. The roles of Ca doped

Despite the similarity among the spatial distribution of the relevant molecular orbitals as shown in Fig. 4, we have noticed two major roles played by Ca atom doped in the Mn cluster: First it is seen from Fig. 9 that the spatial channel of the electron flow of $X = \text{Ca(OH)}_3$ is a little different from that of $X = \text{OH}$, although

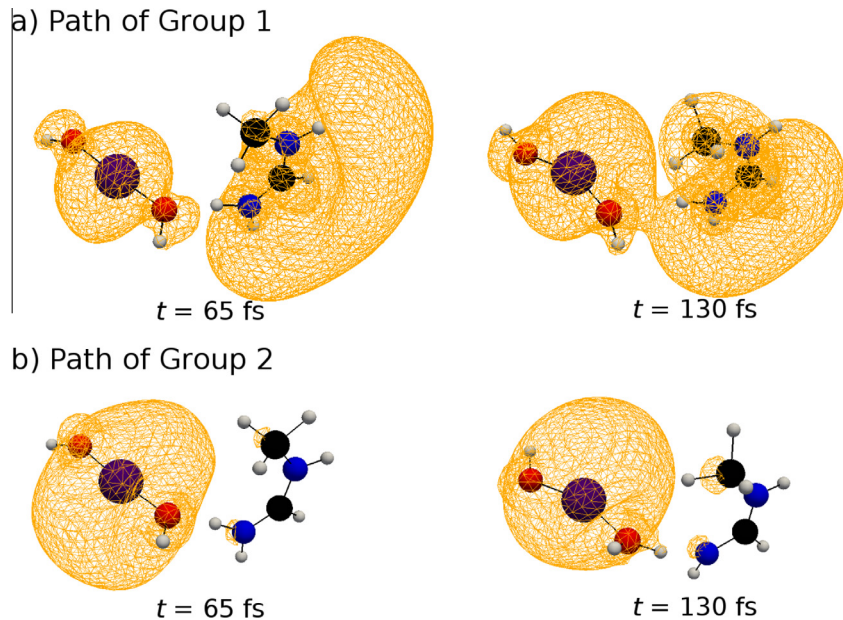


Fig. 12. Snapshots of the spatial distribution of unpaired electron density along the paths of Group 1 (a) and Group 2 (b) for $X = \text{OH}$. Group 2 is dominated by the d-d states, which renders both the H^{T} and electron back to EPA side. While Group 1 represents the asymptotic (well separated) biradical state including the Rydberg-like states and no H^{T} back transfer happens. The path-branching is invoked at $t = 65 \text{ fs}$, and the character of the spatial distribution of the unpaired electrons is preserved even at $t = 130 \text{ fs}$.

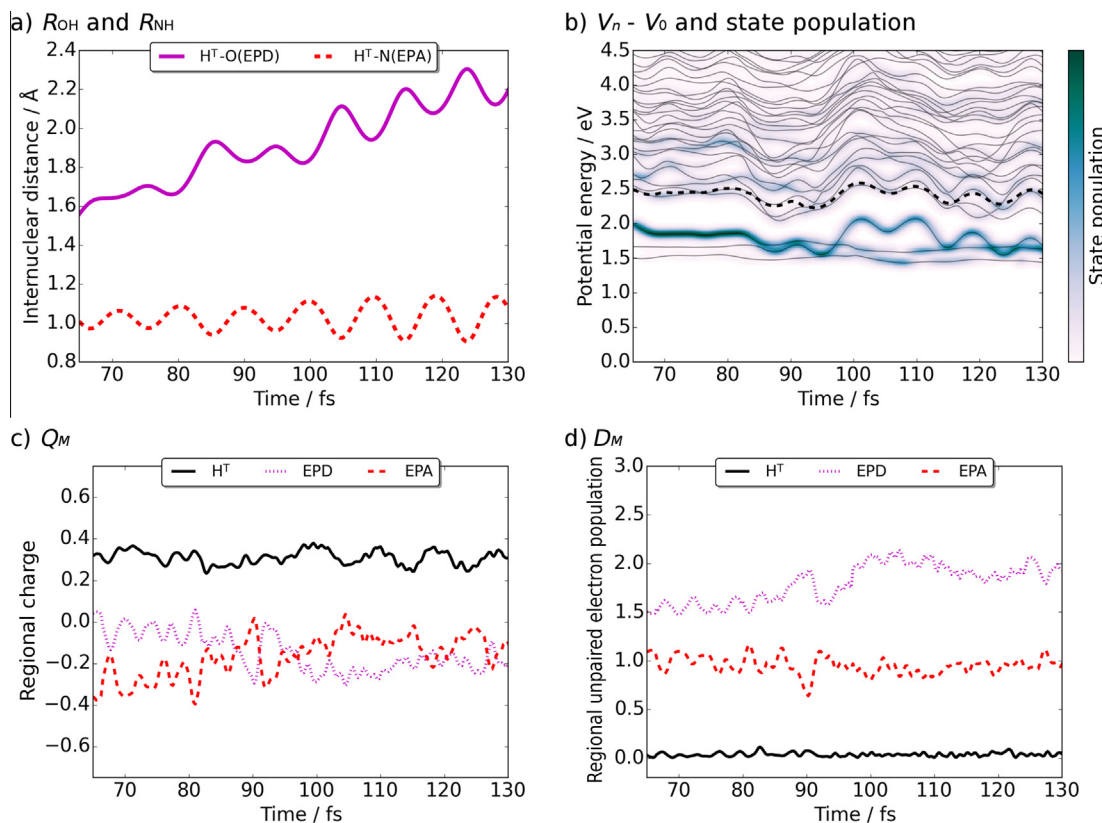


Fig. 13. Selected properties along the path of Group 1, which is dominated by the asymptotic biradical states including the Rydberg-like states for $X = \text{OH}$. The path-branching is invoked at $t = 65 \text{ fs}$.

the mechanism of charge separation is essentially the same. See Fig. 7(b) for R_{OH} and R_{NH} , Fig. 8(b) for adiabatic potential energy and population, Fig. 9(b) for spatial distribution of unpaired electron density, Fig. 10(c) for Q_M , and Fig. 10(d) for D_M to confirm

the similarities between $X = \text{OH}$ and $X = \text{Ca(OH)}_3$. On the other hand, in contrast to the unpaired electrons of $X = \text{OH}$, those of $X = \text{Ca(OH)}_3$ move clockwise (compare panels (a) and (b) in Fig. 9). This is because the unpaired electrons reach EPA passing

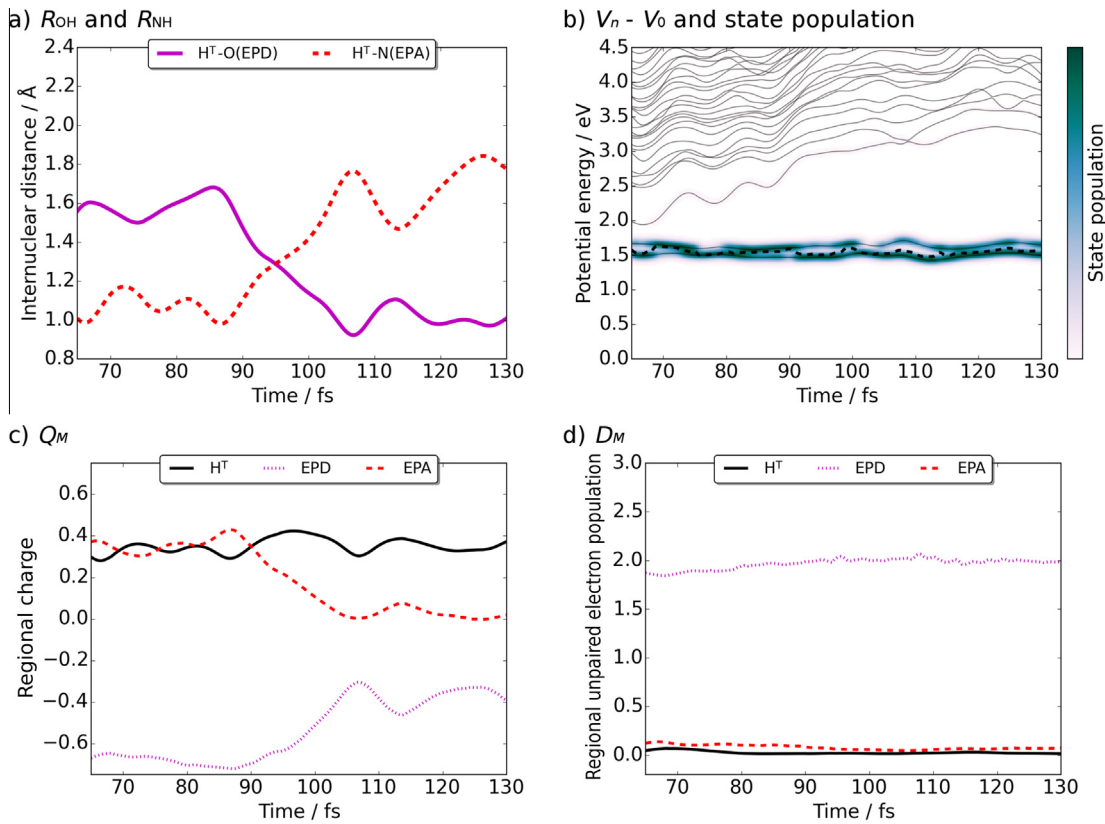


Fig. 14. Selected properties along the path of Group 2, which is dominated by the d-d states for $X = \text{OH}$. The path is the counterpart of the path of Fig. 13 (see Fig. 11 also).

through the Ca atom. Therefore, the doped Ca atom seems to serve to control the channel of electron flow by letting the electrons go through itself.

The second major role of Ca we notice is suggested back in Fig. 8 (b). Compare panels (a) for $X = \text{OH}$ and (b) for $X = \text{Ca(OH)}_3$. Obviously the d-d band states are greatly modulated by the presence of Ca atom. Only one of them stays in the low energy region, which has been lowered than the lowest d-d state in the system of $X = \text{OH}$. Furthermore it turns out as observed clearly in Fig. 8 that the undesirable nonadiabatic transition from CPET state to the d-d band state, which eventually annihilates the created pair of proton and electron, is mostly suppressed. We have conducted several long-time wavepacket propagations following after the CPET process and confirmed that this effect is indeed given by the replacement from $X = \text{OH}$ to $X = \text{Ca(OH)}_3$, although we cannot tell quantitatively how much the deterioration of the CPET is suppressed in this level of calculations. Thus we have found on one hand a physical channel that can hamper the efficient production of the pair of proton and electron, and on the other hand, we also have revealed that the Ca atom doping actually makes this channel very narrow.

4. Concluding remarks

We have proposed the excited-state mechanism of charge separation relevant to the catalytic $\text{Mn-H}_2\text{O}$ systems. Theoretically speaking, it can be simply termed as excited-state coupled proton-electron transfer (CPET) through AX/CI. In CPET, the electron is transferred from the electron-proton donor (EPD) to the Rydberg-like states of the electron-proton acceptor (EPA) through the different pathways of the proton. Various choices of the

functional group X and/or the acceptors A have been examined and found to have this common mechanism. The ground-state dynamics have shown that electron transfer does not occur, even if the ordinary concerted proton transfer does.

To be more precise, proton is shifted from EPD to EPA carrying electrons as much as $(1 - n)e$ without a radical character. The remaining radical electrons of ne flow into the Rydberg-like states of EPA passing through totally different spatial pathways from that of the proton. This induces charge separation composed of $+ne$ and $-ne$ in the excited state of EPA. In the present case study, the charge n is estimated to be 0.4 by Löwdin's method [47], which is less efficient than the classical charge separation consisting of a pair of point charges $+1e$ and $-1e$. Note again however that the perfect charge separation consisting of $+1e$ and $-1e$ demands extremely high energy. Thus it turns out that the presence of the vacant diffused states is critically important for this CPET to be realized in a relatively low-energy condition. Our experience suggests that the Rydberg states of nitrogen atoms compounding EPA (actually the protein residues and ammonia clusters) are the main player of this role.

The mechanism of annihilation of the created pair of proton and electron through the d-d states has been identified by means of the path-branching representation. After the first CPET inducing the charge separation, considerable amount of unpaired electrons created on the Rydberg-like states in EPA are rendered back to EPD site through the d-d states passing through another AX/CI found. Interestingly, Ca(OH)_3 replacing X = OH in EPA site has been found to suppress the dynamics through this inconvenient channel. Besides, the doped Ca atom has been found to control the channel of electron flow by letting the electrons go through itself. This is an example of chemical modification of nonadiabatic transitions.

(See [49–51] for laser modification of conical intersection.) Further study is needed to establish a principle of chemical “control” in order for us to be able to “design” conical intersections.

The proposed mechanisms should lie ubiquitously behind the phenomena of charge separation in chemical and biological systems. A good design of efficient photocatalytic systems should need to take account of the factors, both positive and negative, revealed in the present study. We hope the present study to assist to materialize such efficient catalysts.

On the other hand, we should recall that the above mechanism alone is not responsible for the entire process of Eq. (1), in particular, for the complicated chemical processes leading to generation of oxygen molecules. This does not imply that the present elementally mechanism is not crucial in the photochemistry of water splitting reaction. On the contrary, it is quite likely that any global models trying to comprehend the entire cycle of water oxidation should take a careful account of the present nonadiabatic electron dynamics of excited-state creation of proton–electron pair. We will show such a global model in our forthcoming report [52].

Appendix A. Supplementary data

Supplementary data associated with this article can be found, in the online version, at <http://dx.doi.org/10.1016/j.chemphys.2016.05.021>.

References

- [1] A.L. Sobolewski, W. Domcke, Phys. Chem. Chem. Phys. 14 (2012) 12807–12817.
- [2] X. Liu, A.L. Sobolewski, R. Borrelli, W. Domcke, Phys. Chem. Chem. Phys. 15 (2013) 5957–5966.
- [3] X. Liu, T.N. Karsili, A.L. Sobolewski, W. Domcke, J. Phys. Chem. B 119 (2015) 10664–10672.
- [4] T.N. Karsili, D. Tuna, J. Ehrmaier, W. Domcke, Phys. Chem. Chem. Phys. 17 (2015) 32183–32193.
- [5] X. Liu, T.N. Karsili, A.L. Sobolewski, W. Domcke, Chem. Phys. 464 (2016) 78–85.
- [6] M.D. Kärkä, O. Verho, E.V. Johnston, B. Åkermark, Chem. Rev. 114 (2014) 11863–12001.
- [7] J.R. Galán-Mascarós, ChemElectroChem 2 (2015) 37–50.
- [8] M. Yagi, M. Kaneko, Chem. Rev. 101 (2001) 21–36.
- [9] H. Yamazaki, A. Shouji, M. Kajita, M. Yagi, Coord. Chem. Rev. 254 (2010) 2483–2491.
- [10] P.D. Tran, V. Artero, M. Fontecave, Energy Environ. Sci. 3 (2010) 727–747.
- [11] M.M. Najafpour, T. Ehrenberg, M. Wiechen, P. Kurz, Angew. Chem. Int. Ed. 49 (2010) 2233–2237.
- [12] Y. Umena, K. Kawakami, J.-R. Shen, N. Kamiya, Nature 473 (2011) 55–60.
- [13] M. Shoji, H. Isobe, S. Yamanaka, M. Suga, F. Akita, J.-R. Shen, K. Yamaguchi, Chem. Phys. Lett. 623 (2015) 1–7.
- [14] A. Sobolewski, W. Domcke, C. Dedonder-Lardeux, C. Jouvet, Phys. Chem. Chem. Phys. 4 (2002) 1093–1100.
- [15] A. Carrera, I. Nielsen, P. Carcabal, C. Dedonder, M. Broquier, C. Jouvet, W. Domcke, A. Sobolewski, J. Chem. Phys. 130 (2009) 024302.
- [16] M. Miyazaki, R. Ohara, K. Daigoku, K. Hashimoto, J.R. Woodward, C. Dedonder, C. Jouvet, M. Fujii, Angew. Chem. Int. Ed. 54 (2015) 15089–15093.
- [17] K. Nagashima, K. Takatsuka, J. Phys. Chem. A 116 (2012) 11167–11179.
- [18] T.J. Martínez, Acc. Chem. Res. 39 (2006) 119–126.
- [19] J.D. Coe, B.G. Levine, T.J. Martínez, J. Phys. Chem. A 111 (2007) 11302–11310.
- [20] S. Hammes-Schiffer, Chem. Rev. 110 (2010) 6937–6938.
- [21] R. Daengngern, N. Kungwan, P. Wolschann, A.J. Aquino, H. Lischka, M. Barbatti, J. Phys. Chem. A 115 (2011) 14129–14136.
- [22] S. Hammes-Schiffer, J. Phys. Chem. Lett. 2 (2011) 1410–1416.
- [23] A. Sirjoos Singh, M.V. Pak, S. Hammes-Schiffer, J. Chem. Theory Comput. 7 (2011) 2689–2693.
- [24] A.-P. Gámez-Hernández, A. Magomedov, G. Hummer, V.R. Kaila, J. Phys. Chem. B 119 (2015) 2611–2619.
- [25] P. Goyal, C.A. Schwerdtfeger, A.V. Soudackov, S. Hammes-Schiffer, J. Phys. Chem. B 119 (2015) 2758–2768.
- [26] K. Yamamoto, K. Takatsuka, ChemPhysChem 16 (2015) 2534–2537.
- [27] K. Takatsuka, T. Fueno, K. Yamaguchi, Theor. Chim. Acta 48 (1978) 175–183.
- [28] K. Nagashima, K. Takatsuka, J. Phys. Chem. A 113 (2009) 15240–15249.
- [29] L.I. Schiff, Quantum Mechanics, McGraw-Hill, New York, 1968.
- [30] M. Okuyama, K. Takatsuka, Chem. Phys. Lett. 476 (2009) 109–115.
- [31] I. Barth, H.-C. Hege, H. Ikeda, A. Kenfack, M. Koppitz, J. Manz, F. Marquardt, G.K. Paramonov, Chem. Phys. Lett. 481 (2009) 118–123.
- [32] J. Manz, J.F. Pérez-Torres, Y. Yang, J. Phys. Chem. A 118 (2014) 8411–8425.
- [33] M. Okuyama, K. Takatsuka, Bull. Chem. Soc. Jpn. 85 (2012) 217–227.
- [34] T. Bredtmann, D.J. Diestler, S.-D. Li, J. Manz, J.F. Pérez-Torres, W.-J. Tian, Y.-B. Wu, Y. Yang, H.-J. Zhai, Phys. Chem. Chem. Phys. 17 (2015) 29421–29464.
- [35] H. Ushiyama, K. Takatsuka, Angew. Chem. 119 (2007) 593–596.
- [36] K. Takatsuka, J. Phys. Chem. A 111 (2007) 10196–10204.
- [37] T. Yonehara, K. Takatsuka, J. Chem. Phys. 129 (2008) 134109.
- [38] K. Takatsuka, Int. J. Quantum Chem. 109 (2009) 2131–2142.
- [39] K. Takatsuka, T. Yonehara, Adv. Chem. Phys. 144 (2010) 93–156.
- [40] K. Takatsuka, T. Yonehara, Phys. Chem. Chem. Phys. 13 (2011) 4987–5016.
- [41] T. Yonehara, K. Hanasaki, K. Takatsuka, Chem. Rev. 112 (2012) 499–542.
- [42] K. Yamamoto, K. Takatsuka, J. Chem. Phys. 140 (2014) 124111.
- [43] K. Takatsuka, T. Yonehara, K. Hanasaki, Y. Arasaki, Chemical Theory Beyond the Born–Oppenheimer Paradigm: Nonadiabatic Electronic and Nuclear Dynamics in Chemical Reactions, World Scientific, 2015.
- [44] M.W. Schmidt, K.K. Baldridge, J.A. Boatz, S.T. Elbert, M.S. Gordon, J.H. Jensen, S. Koseki, N. Matsunaga, K.A. Nguyen, S. Su, T.L. Windus, M. Dupuis, J.A. Montgomery, J. Comput. Chem. 14 (1993) 1347–1363.
- [45] M.S. Gordon, M.W. Schmidt, Theory and Applications of Computational Chemistry: the first forty years, Elsevier, Amsterdam, 2005. pp. 1167–1189.
- [46] W.J. Stevens, M. Krauss, H. Basch, P.G. Jasien, Can. J. Chem. 70 (1992) 612–630.
- [47] P.-O. Löwdin, J. Chem. Phys. 18 (1950) 365–375.
- [48] R.S. Mulliken, J. Chem. Phys. 23 (1955) 1833–1840.
- [49] Y. Arasaki, K. Takatsuka, Phys. Chem. Chem. Phys. 12 (2010) 1239–1242.
- [50] Y. Arasaki, K. Takatsuka, Phys. Chem. Chem. Phys. 13 (2011) 4756–4758.
- [51] Y. Arasaki, K. Wang, V. McKoy, K. Takatsuka, Phys. Chem. Chem. Phys. 13 (2011) 8681–8689.
- [52] K. Yamamoto, K. Takatsuka, to be published.



Kento Yamamoto was born in Osaka, Japan. He earned his B.Sc. from Kwansei Gakuin University in 2009, and received his Ph.D. in Chemistry from the University of Tokyo in 2015 under the supervision of Prof. Kazuo Takatsuka. He is currently a postdoctoral fellow at the Fukui Institute for Fundamental Chemistry. His current interests include nonadiabatic electron dynamics relevant to photocatalytic water-splitting reactions.



Kazuo Takatsuka was born in Takayama, Japan and received Dr. of Engineering Science from Osaka University in 1978. After postdoctoral works at North Dakota State University (Prof. Mark Gordon) and Caltech (Prof. Vincent McKoy), he joined Institute of Molecular Science, Japan. In 1992 he started to serve as a professor for Nagoya University, and moved to the University of Tokyo in 1997. He retired from this university in 2016 as a professor emeritus. Then he has joined the Fukui Institute for Fundamental Chemistry, Kyoto University, Japan as Research Leader. His current interests are in the theory of electronic and nuclear dynamics beyond the Born–Oppenheimer framework, nuclear wavepacket dynamics with pump-probe photoelectron spectroscopy, nonadiabatic electron wavepacket dynamics in chemical reactions, theory of chemical dynamics in condensed phases, many-body semiclassics, chaos and nonlinear dynamics in atomic clusters, semiclassical quantization of chaos, dynamics of morphology, and so on.